Enhanced cooperativity in supported spin-crossover metal-organic frameworks

Thomas Groizard,[†] Nick Papior,[‡] Boris Le Guennic,[†] Vincent Robert,[¶] and Mikaël Kepenekian[*,†]

†*Institut des Sciences Chimiques de Rennes (ISCR), Université de Rennes 1, CNRS, UMR 6226, 35042 Rennes, France*

‡*ICN2 - Institut Catala de Nanociencia i Nanotecnologia, Campus UAB, 08193 Bellaterra (Barcelona), Spain*

¶*Laboratoire de Chimie Quantique, Université de Strasbourg, CNRS, UMR 7177 Strasbourg, France*

E-mail: mikael.kepenekian@univ-rennes1.fr

Abstract

The impact of surface deposition on cooperativity is explored in Au(111) supported self-assembled metal-organic frameworks (MOF) based on Fe(II) ions. Using a thermodynamic model, we first demonstrate that dimensionality reduction combined with deposition on a metal surface are likely to deeply enhance the spin-crossover cooperativity, going from $\gamma_{3D} = 16$ K for the bulk material to $\gamma_{2D}^{supp} = 386$ K for its 2D supported derivative. Based on density functional theory, we then elucidate the electronic structure of a promising Fe-based MOF. A chemical strategy is proposed to turn a weakly interacting magnetic system into a strongly cooperative spin-crossover monolayer with $\gamma_{MOF}^{Au(111)} = 83$ K. These results open a promising route to the fabrication of cooperative materials based on SCO Fe(II) platforms.

Graphical TOC Entry

TOC ENTRY REQUIRED

Table of Contents Graphical Abstract

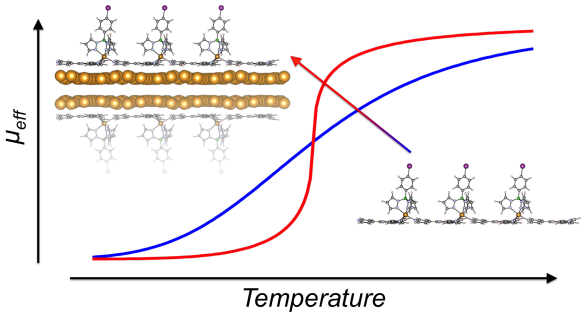

Molecular electronics originally proposed in the 1950s and reinvigorated by the founding proposition of Aviram and Ratner[1] has led to intense activity on the study of electronic transport through single molecules, supported by the advent of scanning tunneling microscopy (STM) and break junction setups.[2,3] More recently, molecules entered the field of spintronics, *i.e.* the control and manipulation of spins,[4] and gave birth to molecular spintronics.[5–8] Whereas single molecule magnets (SMM) display bistability at rather low temperatures,[9,10] higher temperature regimes are reached for spin-crossover (SCO) materials.[11]

In order to bridge the gap between functional molecules and practical devices, one has to deposit the objects on a surface while retaining the bistability property. With respect to the intense activity in the field of adsorbed SMM,[8,12–15] SCO supported compounds have received much less attention. It is only recently that supported examples have emerged, starting from 3D materials with thin-films grown on gold.[11,16,17] 0D systems followed based on single SCO molecules,[18–24] or molecular junctions.[25] However, 2D monolayer organized networks exhibiting SCO behavior have not been reported so far. Not only should low-dimensional SCO patterns offer new insights into the spin transition phenomenon, but such organized networks may also offer the opportunity to control the intermolecular interactions dictating the collective behavior of transiting centers (*a.k.a.* cooperativity).[26]

With this goal in mind, a promising route might come from the use of self-assembled MOF.[27] Indeed, exchange couplings[28] were reported in several 2D MOF based on $3d$ ions such as Fe,[29,30] Ni,[31] Mn[32,33] or Cu.[34] Recently, Umbach *et al.* have investigated a Au(111)-supported MOF based on Fe(II) ions and 2,4,6-tris(4-pyridyl)-1,3,5-triazine (T4PT) ligand.[30] Interestingly, in addition to the observation of a weakly ferromagnetic behaviour, the speculated structure of the system consists in FeN_6 units, an archetype arrangement of SCO systems.[35]

In this letter, we use a model based on Fe(II) transiting unit to investigate the effect of dimensionality reduction and surface deposition. Our thermodynamic model shows that a metallic substrate is likely to enhance cooperativity by an order of magnitude. In the

light of these findings, we then perform calculations based on density functional theory (DFT) to establish the structure of the synthetic Fe-T4PT MOF supported on a Au(111) surface.[30] We show that the most stable structure consists of FeN_3Au_3 units rather than on the expected FeN_6 building blocks. Beyond the interpretation of experimental results, a chemical modification of the ligand is proposed to generate a FeN_6 candidate for spin-crossover behavior. Finally, we demonstrate that the Au(111) surface is likely to drive the original weakly-coupled system into a highly cooperative material.

From a thermodynamic point of view, the low-spin (LS) to high-spin (HS) transition displays an overall entropy increase resulting from (i) the spin change (from LS, S = 0 to HS, S = 2 in the case of Fe(II) ions), and (ii) the weakening of the metal-ligand bond strength (vibrational contribution). As a consequence, for the transition to occur the enthalpy change must be positive as well. This quantity can be approximated by the electronic adiabatic energy difference ΔE_{adia}, *i.e.* the energetic difference between the HS and LS states each taken at its optimized geometry. It is accessible from quantum chemistry calculations. Naturally, weak fields that favor HS over LS as the ground-state are not suitable for SCO. In the same way, too strong fields will lead to a blocked LS state. For Fe(II)-based compounds, ΔE_{adia} is traditionally of the order of 100 meV when room-temperature transition is observed.

The steepness of the transition phenomenon is characteristic of the extent of cooperativity, a much more difficult quantity to retrieve from calculations. Indeed, interactions between transiting units can be mediated by phonon coupling, electron-phonon coupling[36,37] and driven by the Madelung field modulation in the crystal.[26,38]

In the following, we intend to inspect changes in charge distribution resulting from dimensionality reduction and surface deposition. Thus, let us briefly recall the so-called polarization contribution.[38] In a mean-field scheme, the molar Gibbs free energy G of a mixture of spin transiting centers as a function of the HS molar fraction x reads

$$G(x,T) = G_{ni} - TS_{mix} + G_{pol}$$

where $G_{ni} = xG_{HS} + (1-x)G_{LS}$ is the free energy of non-interacting sites. S_{mix} is the entropy of mixing $-R(x\ln(x)+(1-x)\ln(1-x))$. G_{pol} arises from the electrostatic potentials generated by the rest of the transiting sites and possibly the metallic surface at the position of (i) Fe ions (V_{LS}, V_{HS}), and (ii) ligands (v_{LS}, v_{HS}).[26,38] This contribution G_{pol} to the Gibbs free energy reads :

$$G_{pol} = \gamma x(1-x)$$
$$\text{with } \gamma = \Delta Q(\delta V_{HS} - \delta V_{LS})$$

where $\Delta Q = Q_{HS} - Q_{LS}$ is the charge variation on the Fe center. δV_{HS} and δV_{LS} are the potential differences between metal and ligand positions in the HS and LS state, respectively.

In order to modulate the dimensionality of the materials, let us consider a model system consisting in neutral Fe(II) units in a typical N_6 environment. $Fe(NCH)_4(NCS)_2$ units are formed from a formally Fe^{2+} ion surrounded by four neutral NCH and two thiocyanate NCS^- ligands. Charges are extracted from *ab initio* calculations,[26] and summarized in Table 1 along with the geometrical parameters defining the hypothetical 3D cubic crystal structure.

Table 1: Fe-Fe and Fe-N distances (in Å) of the cubic model structure of built with $Fe(NCH)_4(NCS)_2$ units, and corresponding point charges (atomic units) on Fe (Q) and ligands (q) for both LS (S = 0) and HS (S = 2) states.[26]

Spin state	d(Fe-Fe)	d(Fe-N)	Q	q_N	q_{NCS}
LS	11.75	2.00	+1.44	-0.18	-0.36
HS	12.00	2.20	+1.92	-0.24	-0.48

Starting from such a $Fe(NCH)_4(NCS)_2$ unit, we built three different environments. First, we considered a 3D network, then a free-standing network, and finally a 2D network supported on a metallic surface. ΔE_{adia} and ΔS are chosen to establish a critical temperature $T_{1/2}$ equal to 200 K. Let us stress that these parameters naturally affect the shape of the transition but not the γ value. From the values given in Table 1, the 3D network exhibits a

weak cooperativity with $\gamma_{3D} = 16$ K and a smooth transition is observed (Figure 1).

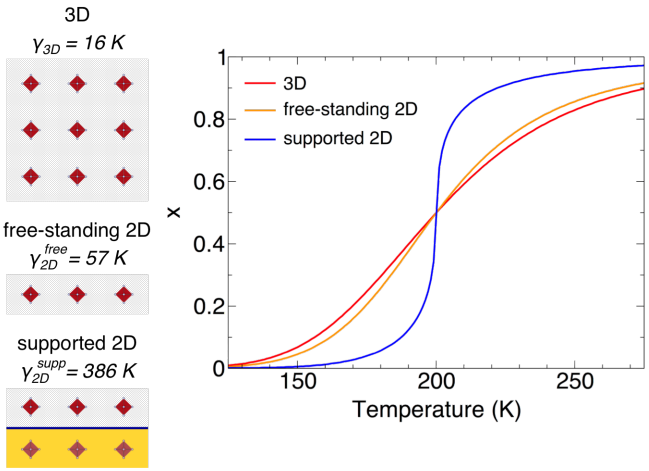

Figure 1: Simulated temperature-induced spin-crossover for the model FeN_6 units organized in (i) a 3D network, (ii) a free-standing 2D network, and (iii) a 2D network supported on a metallic surface generating mirror charges. ΔE_{adia} is 140 meV and ΔS is set to 0.70 meV/K leading to a critical temperature $T_{1/2}$ of 200 K. Deposition on a surface leads to a large increase of the polarization-induced cooperativity and, thus, to a more abrupt transition.

Upon 3D to 2D dimension reduction, the cooperativity is moderately increased by a factor of 3.5 with $\gamma_{2D}^{\text{free}} = 57$ K. Formally, half of the point charges generating the Madelung field were set to zero when moving to this free standing 2D network. The presence of a metallic surface is likely to change this state of affairs. From elementary electrostatics, each charge above the equipotential metallic surface generates a mirror charge within the bulk. Quite remarkably, the cooperativity parameter is enhanced to $\gamma_{2D}^{\text{supp}} = 386$ K. As a main conclusion, the polarization induced by the proximity of a metallic surface drives the system into a highly cooperative regime, featured by an amplification factor $\gamma_{2D}^{\text{supp}}/\gamma_{3D}$ for cooperativity larger than 20.

Naturally, our model is likely to exaggerate polarization effects. Indeed, the limited size of the ligands concentrates the charge variation, with respect to more realistic ligands, and therefore might artificially amplify the role of the surface. To support these findings on a simplified model, we then assessed its robustness with a synthetic Fe(II)-based MOF self-assembled on Au(111).[30] First, structural and electronic information are explored from DFT calculations. Out of atomically resolved STM topographic images, Umbach *et al.* have

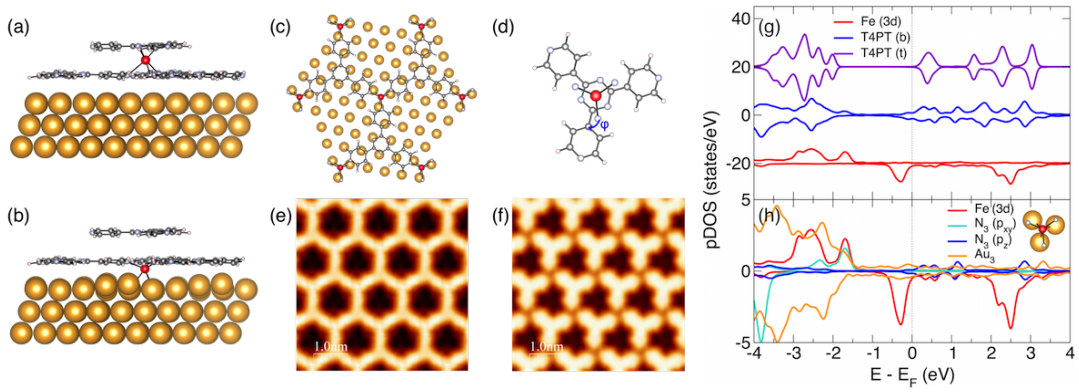

Figure 2: (a) Side view of the starting geometry for Fe-T4PT on top of Au(111). Each Fe(II) ion is bound to three T4PT molecules of the bottom layer and a supplementary T4PT from the top layer. Fe(II) ions lie above the bottom organic layer. Au, Fe, N, C and H atoms are depicted in yellow, red, blue, gray and pale pink, respectively. (b) Side view of the DFT optimized geometry. Fe(II) ions move into Au(111) hollow sites. (c) Top view of the Fe-T4PT bottom layer. (d) Top view of the second T4PT layer. For clarity, the Fe center and the bonded N atoms are displayed. The top T4PT molecule forms an angle $\phi = 26°$ with the first layer. Simulated constant current STM images at (e) 0.10 V and (f) 2.0 V. (g) pDOS on the Fe 3d orbitals (red line), the bottom T4PT layer (blue) and the top T4PT layer (violet). The top T4PT layer does not exhibit any hybridization. (h) pDOS on Fe 3d orbitals (red), on $2p_x$ and $2p_y$ orbitals of the N atoms of the T4PT bottom layer neighboring Fe (blue) and the neighboring Au atoms (orange) that form the hollow site occupied by the Fe(II) ion (red). The inset shows the iron ion and its coordination sphere.

been able to propose a structure for the monolayer formed from the sublimation of T4PT molecules and Fe atoms.[30] It consists in three μ^1-T4PT ligands pointing at one Fe(II) ion and a second layer of η^3-T4PT ligands with the central triazine moiety of T4PT lying on top of the iron center. However, the optimized structure unambiguously leads to a different scenario. The Fe(II) ion moves away from the second organic layer and occupies a hollow site of the Au(111) surface (Figure 2-b-d) with Fe-Au distances of 2.76 Å, Fe-N bond lengths of 2.14 Å with the bottom layer (see Figure S1 and Table S1 in Supporting Information), while the Fe-N distances with the second triazine layer are larger than 4 Å. Therefore, the system does not present itself as an expected octahedral FeN_6 coordination sphere but rather as a trigonal prismatic $FeAu_3N_3$ one. Trigonal prismatic geometry is well known in Fe(II) complexes. In particular, it is often observed when a geometric constraint is imposed, *e.g.* by macrocycle ligands.[39,40] Here, the constraints is imposed by the periodicity of the hybrid network (Fe-T4PT and Au(111)). This optimized structure leads to STM simulated images

that compare well with the experimental ones (Figure 2-e,f).[30] A low bias constant current image highlights the first layer, while a higher bias reveals the position of the second layer.

The computed Bader charge for Fe (+1.76 e^-) is compatible with a +II formal oxidation state. This is confirmed by the analysis of the density of states (DOS, Figure 2-g). The iron levels are typical of a HS Fe(II) ion with five electrons occupying the spin-up $3d$ levels, while a single one lies in the spin-down $3d$ levels. This picture is also supported by X-ray absorption spectroscopy (XAS) and X-ray magnetic circular dichroism (XMCD) measurements.[30] Around this cationic center, the top T4PT layer shows typical molecular levels with no hybridization either with the bottom organic layer or the metallic center. On the other hand, the bottom layer shows large hybridization with a modest charge transfer (0.28 e^-) to the lowest unoccupied molecular orbital (LUMO). The energy ordering is also characteristic of a trigonal prismatic N_3Au_3 ligand field with the HS state more stable by 1.52 eV than the LS solution and the intermediate state (S = 1) lying much higher in energy. Therefore, the electronic structure of the Fe(II) ion is best described by a weak trigonal prismatic ligand field formed by three Au neighboring atoms and three terminal N atoms of the T4PT bottom layer.

Our description is further confirmed by the inspection of magnetic properties. Indeed, Figure S1-a shows the calculated ground-state spin-density of the Fe-T4PT network on Au(111), suggesting parallel alignement of spins localized on Fe ions. XMCD measurements have indeed shown a weak ferromagnetic coupling between iron centers, featuring a critical temperature T_c of 1.8 K.[30] Based on the optimized structure, we performed a detailed inspection of the magnetic coupling (see Supporting Information for the complete description of our investigation) that reveals the respective roles of the surface-mediated RKKY interaction and of the T4PT linker. The resulting ferromagnetic coupling $J = 0.51$ K is in agreement with experimental findings strengthening our conviction that our description of the electronic structure is correct.

At this stage, the negative energy difference between HS and LS states (ΔE_{adia} = -

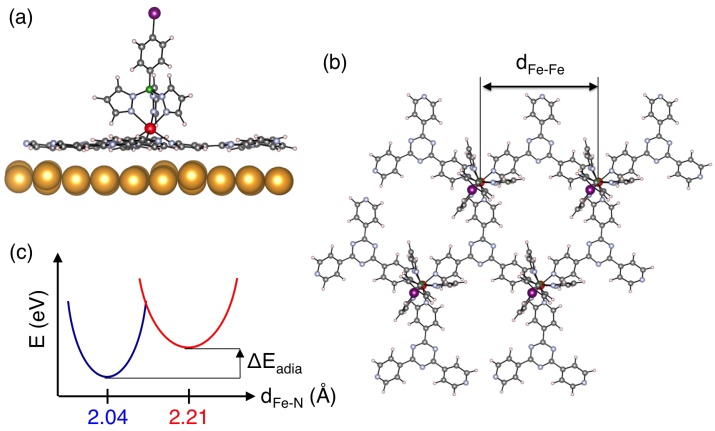

Figure 3: (a) Optimized structure of Fe(T4PT)(p-IC_6H_4)$B(pz)_3$ on Au(111). For clarity, only one gold layer is displayed. (b) Top view of the optimized free-standing Fe(T4PT)(p-IC_6H_4)$B(pz)_3$ network. The Fe-Fe distance is optimized with respect to the spin value. (c) Schematic energetics, ΔE_{adia} is positive, a prerequisite for spin-crossover.

1.52 eV) is not compatible with SCO behaviour. Thus, the prerequisites for the generation of bistable devices are definitely not fulfilled. However, our calculations show that the T4PT top layer is only weakly bound to the bottom one and therefore can be substituted by other molecules with stronger binding energy to the Fe(II) ion. We felt that chemical modification of the organic part might restore the N_6 coordination sphere around the Fe(II) centers and shift ΔE_{adia} to positive values. Indeed, molecular magnetism has produced a wealth of ligands with the ability to modulate the energetics. Then, we intended to examine the impact of surface deposition of the modified Fe(II)-based MOF. Here, we restrict our study to two tridentate N-terminated ligands. As a first guess, we consider the 1,4,7-trimethyl-1,4,7-triazacyclononane (tacn) ligand, known to generate Fe(II) compounds exhibiting temperature-induced SCO.[41] As hopped, the iron center leaves the gold hollow site and a N_6 coordination sphere is restored after DFT geometry optimization. A similar picture holds for tris(pyrazolyl)-borate (p-IC_6H_4)$B(pz)_3$ ligand (Figure 3-a), a well-known negatively-charged ligand in SCO chemistry.[42,43]

In this first step, we have conserved the original periodicity of the network imposed by the commensuration with the Au(111) surface. In that configuration, Fe-T4PT distances ($\approx$ 2.15 Å) are too large to stabilize the LS state. However, since the Fe ion is not bound to the

Au hollow site anymore and that the T4PT is weakly adsorbed to the substrate, there is no reason for the MOF to conserve the same periodicity. From a computational perspective, it is not affordable to vary the periodicity of the MOF network while keeping the gold substrate fixed. Thus, we considered the free-standing Fe(T4PT)(tacn) and Fe(T4PT)(p-IC_6H_4)$B(pz)_3$ 2D structures and optimized the atomic positions as well as the unit cell vectors (Figure 3-b) for the HS and LS states.

Unfortunately, a negative adiabatic energy difference $\Delta E_{\text{adia}} = -340$ meV is calculated for the tacn ligand. Thus, the HS state remains the ground-state and no SCO behavior can be anticipated. A contrasted scenario is observed when T4PT is substituted by (p-IC_6H_4)$B(pz)_3$. The adiabatic energy difference is much reduced and remains positive, ΔE_{adia} =140 meV (Figure 3-c). Meanwhile, the equilibrium geometries are characterized by a Fe-N average distance that varies from 2.04 Å (LS) to 2.21 Å (HS) along with a 0.31 Å elongation of the Fe-Fe distance (12.45 to 12.76 Å). All these values are compatible with a typical SCO behavior and the parameters used in the model previously presented (see Table 1).

In order to evaluate the charge redistribution, the network must be placed on top of the Au(111) surface. As the periodicities of both patterns now differ, we used a single unit consisting of one Fe center and its coordination sphere, *i.e.* three T4PT and one (p-IC_6H_4)$B(pz)_3$ ligands, on top of a large gold layer. Out of Bader analysis, the charge redistribution on the Fe center along the transition is calculated $\Delta Q = 0.64$ e^-. This value is in agreement with the ones estimated[44] and calculated on molecular FeN_6 SCO compounds.[26,45] The polarization contribution was then evaluated by using (i) the atomic positions of the free-standing structure, and (ii) the point charges previously determined. The cooperativity parameter γ_{MOF} is found 20 K. This rather weak value in the 3D material is suggestive of a smooth transition phenomenon. In the presence of the metallic gold surface, a $\gamma_{\text{MOF}}^{\text{Au(111)}} = 83$ K value is calculated. Therefore, one can anticipate a much more abrupt transition, the amplification factor $\gamma_{\text{MOF}}^{\text{Au(111)}}/\gamma_{\text{MOF}}$ reaching a noticeable value of 4.15 for a very realistic synthetic system. Our initial model $Fe(NCH)_4(NCS)_2$ is attractive from its compact

form, but may overestimate actual charge reorganizations along spin transition. However, it provides a transferable view on the impact of surface deposition in the suggested Fe(II) T4PT derivative.

In this work, the prime role played by surfaces in the generation of strongly cooperative SCO compounds is established. The extension of a thermodynamic model stresses the importance of the deposition of FeN_6 units on metal substrates. We estimated an enhancement of the cooperativity parameter by a factor larger than 20. To support these views, DFT calculations were performed on a reported MOF supported on a Au(111) surface. The geometry and electronic structure of Fe-T4PT network were characterized and concluded on a HS ground-state excluding any SCO behavior. Nevertheless, we identified a promising (*p*-IC_6H_4)$B(pz)_3$ ligand to construct a spin transiting Au-supported MOF. Quite remarkably, such substitution allows one to satisfy a positive and small enough value (140 meV) for the enthalpy change. Based on this chemical modification, we showed that the deposition on a gold surface induces a significant enhancement of the cooperativity factor. Naturally, our compact model leaves aside various contributions (phonons, solvents, etc.) that are expected to impact on the spin-transition phenomenon and could be advantageously improved in the future.[46] But the polarization part of cooperativity unambiguously benefits from metal deposition. With the ability to increase cooperativity in a rational way, we believe that supported spin-crossover Fe(II) materials open up a promising route in the long-hoped design of hysteresis behavior. This inspection paves the way to the preparation of supported materials to complement the immense chemical strategies that have been developed in the last three decades.

Computational details

DFT calculations are conducted with the SIESTA code.[47,48] The non-local van der Waals density functional (vdW-DF) of Dion *et al.* corrected by Klimeš *et al.* has been used.[49,50] The dipole induced by the adsorption of molecules on the gold surface is treated with the

dipole correction as implemented in SIESTA.[51] The lack of electron correlation is accounted for through the DFT+U approach following Dudarev's scheme.[52] Here, we use a value of $U_{\text{eff}} = 2.0$ eV for Fe atom $3d$ orbitals. This value is compatible with previous inspection of SCO materials.[53] We checked that the amplitude of this energy difference is only slightly modified (less than 0.1 eV) when the the U_{eff} parameter in DFT calculations is varied from 1.0 eV up to 4.0 eV. Core electrons are described with Troullier-Martins pseudopotentials.[54] The valence wavefunction is developed over a double-ζ polarized basis set of finite-range numerical pseudoatomic orbitals.[55]

We rationalize the experimental structure observed by STM images,[30] as a $(\sqrt{21} \times \sqrt{21})$R10.9° unit cell on top of Au(111) containing one Fe atom, one T4PT ligand in the first layer and a second one forming the second layer (Figure 2). We consider the same unit cell with 3 gold layers and a vacuum region of 20 Å. Along the ionic relaxations, the positions of only the 2 top layers are allowed to move until forces are smaller than 0.02 eV/Å, to ensure a bulk-like structure for the bottom layers. The Brillouin zone is integrated using a 3×3×1 Monkhorst-Pack mesh. STM topographic images have been simulated using the Tersoff-Hamman theory[56,57] as implemented by Lorente and coworkers.[58] Charge transfers have been calculated using a Bader charge analysis.[59,60]

In order to check our results, we have repeated all calculations using the VASP code (see Supporting Information for computational details).[61] This different approach has corroborated our conclusions. The Fe-T4PT/Au(111) structure remains similar with a $FeAu_3N_3$ coordination sphere and a similar adiabatic gap ($^{\text{VASP}}\Delta E_{\text{adia}} = -1.58$ eV, *vs.* $^{\text{SIESTA}}\Delta E_{\text{adia}} = -1.52$ eV). It is also the case for Fe(T4PT)(p-IC_6H_4)B(pz)$_3$ with $^{\text{VASP}}\Delta E_{\text{adia}} = 120$ meV, to be compared with $^{\text{SIESTA}}\Delta E_{\text{adia}} = 140$ meV.

Acknowledgements

M. K. work is supported by Rennes Métropole through the *Allocation d'installation scientifique* program. N. P. acknowledges financial support from EU H2020 project no. 676598, "MaX: Materials

at the eXascale" Center of Excellence in Supercomputing Applications. We thank L. Norel, J.-F. Halet, G. Chastanet and N. Lorente for stimulating discussions.

References

(1) Aviram, A.; Ratner, M. A. Molecular Rectifiers. *Chem. Phys. Lett.* **1974**, *29*, 277–283.

(2) Joachim, C.; Gimzewski, J. K.; Aviram, A. Electronics Using Hybrid-molecular and Mono-molecular Devices. *Nature* **2000**, *408*, 541–548.

(3) Sun, L.; Diaz-Fernandez, Y. A.; Gschneidtner, T. A.; Westerlund, F.; Lara-Avila, S.; Moth-Poulsen, K. Single-molecule Electronics: From Chemical Design to Functional Devices. *Chem. Soc. Rev.* **2014**, *43*, 7378–7411.

(4) Zutić, I.; Fabian, J.; Das Sarma, S. Spintronics: Fundamentals and Applications. *Rev. Mod. Phys.* **2004**, *76*, 323–410.

(5) Bogani, L.; Wernsdorfer, W. Molecular Spintronics Using Single-molecule Magnets. *Nature Mater.* **2008**, *7*, 179–186.

(6) Camarero, J.; Coronado, E. Molecular vs. Inorganic Spintronics: The Role of Molecular Materials and Single Molecules. *J. Mater. Chem.* **2009**, *19*, 1678–1684.

(7) Sanvito, S. Molecular Spintronics. *Chem. Soc. Rev.* **2011**, *40*, 3336–3355.

(8) Aradhya, S. V.; Venkataraman, L. Single-molecule Junctions Beyond Electronic Transport. *Nature Nanotech.* **2013**, *8*, 399–410.

(9) Sessoli, R.; Gatteschi, D.; Caneschi, A.; Novak, M. A. Magnetic Bistability in a Metal-Ion Cluster. *Nature* **1993**, *365*, 141–143.

(10) Gatteschi, D.; Sessoli, R.; Villain, J. *Molecular Nanomagnets*; Oxford University Press, 2006.

(11) Bousseksou, A.; Molnár, G.; Salmon, L.; Nicolazzi, W. Molecular Spin Crossover Phenomenon: Recent Achievements and Prospects. *Chem. Soc. Rev.* **2011**, *40*, 3313–3335.

(12) Burgert, M.; Voss, S.; Herr, S.; Fonin, M.; Groth, U.; Rüdiger, U. Single-Molecule Magnets: A New Approach To Investigate the Electronic Structure of Mn_{12} Molecules by Scanning Tunneling Spectroscopy. *J. Am. Chem. Soc.* **2007**, *129*, 14362–14366.

(13) Gonidec, M.; Biagi, R.; Corradini, V.; Moro, F.; De Renzi, V.; del Pennino, U.; Summa, D.; Muccioli, L.; Zannoni, C.; Amabilino, D. B.; Veciana, J. Surface Supramolecular Organization of a Terbium(III) Double-Decker Complex on Graphite and its Single Molecule Magnet Behavior. *J. Am. Chem. Soc.* **2011**, *133*, 6603–6612.

(14) Cornia, A.; Mannini, M.; Sainctavit, P.; Sessoli, R. Chemical Strategies and Characterization Tools for the Organization of Single Molecule Magnets on Surfaces. *Chem. Soc. Rev.* **2011**, *40*, 3076–3091.

(15) Scott, G. D.; Natelson, D. Kondo Resonances in Molecular Devices. *ACS Nano* **2010**, *4*, 3560–3579.

(16) Félix, G.; Abdul-Kader, K.; Mahfoud, T.; Gural'skiy, I. A.; Nicolazzi, W.; Salmon, L.; Molnár, G.; Bousseksou, A. Surface Plasmons Reveal Spin Crossover in Nanometric Layers. *J. Am. Chem. Soc.* **2011**, *133*, 15342–15345.

(17) Pronschinske, A.; Chen, Y.; Lewis, G. F.; Shultz, D. A.; Calzolari, A.; Buongiorno Nardelli, M.; Dougherty, D. B. Modification of Molecular Spin Crossover in Ultrathin Films. *Nano Lett.* **2013**, *13*, 1429–1434.

(18) Miyamachi, T.; Gruber, M.; Davesne, V.; Bowen, M.; Boukari, S.; Joly, L.; Scheurer, F.; Rogez, G.; Yamada, T. K.; Ohresser, P.; Beaurepaire, E.; Wulfhekel, W. Robust Spin Crossover and Memristance Across a Single Molecule. *Nat. Commun.* **2012**, *3*, 938.

(19) Warner, B.; Oberg, J. C.; Gill, T. G.; El Hallak, F.; Hirjibehedin, C. F.; Serri, M.; Heutz, S.; Arrio, M.-A.; Sainctavit, P.; Mannini, M.; Poneti, G.; Sessoli, R.; Rosa, P. Temperature- and Light-Induced Spin Crossover Observed by X-ray Spectroscopy on Isolated Fe(II) Complexes on Gold. *J. Phys. Chem. Lett.* **2013**, *4*, 1546–1552.

(20) Bernien, M.; Naggert, H.; Arruda, L. M.; Kipgen, L.; Nickel, F.; Miguel, J.; Hermanns, C. F.; Krüger, A.; Krüger, D.; Schierle, E.; Weschke, E.; Tuczek, F.; Kuch, W. Highly Efficient Thermal and Light-Induced Spin-State Switching of an Fe(II) Complex in Direct Contact with a Solid Surface. *ACS Nano* **2015**, *9*, 8960–8966.

(21) Gueddida, S.; Gruber, M.; Miyamachi, T.; Beaurepaire, E.; Wulfhekel, W.; Alouani, M. Exchange Coupling of Spin-Crossover Molecules to Ferromagnetic Co Islands. *J. Phys. Chem. Lett.* **2016**, *7*, 900–904.

(22) Beniwal, S.; Zhang, X.; Mu, S.; Naim, A.; Rosa, P.; Chastanet, G.; Létard, J.-F.; Liu, J.; Sterbinsky, G. E.; Arena, D. A.; Dowben, P. A.; Enders, A. Surface-induced Spin State Locking of the $[Fe(H_2B(pz)_2)_2(bipy)]$ Spin Crossover Complex. *J. Phys.: Condens. Matter* **2016**, *28*, 206002.

(23) Bairagi, K. et al. Molecular-scale Dynamics of Light-induced Spin Cross-over in a Two-dimensional Layers. *Nat. Commun.* **2016**, *7*, 12212.

(24) Jasper-Tönnies, T.; Gruber, M.; Karan, S.; Jacob, H.; Tuczek, F.; Berndt, R. Deposition of a Cationic Fe^{III} Spin-Crossover Complex on Au(111): Impact of the Counter Ion. *J. Phys. Chem. Lett.* **2017**, *8*, 1569–1573.

(25) Meded, V.; Bagrets, A.; Fink, K.; Chandrasekar, R.; Ruben, M.; Evers, F.; Bernand-Mantel, A.; Seldenthuis, J. S.; Beukman, A.; van der Zant, H. S. J. Electrical Control Over the Fe(II) Spin Crossover in a Single Molecule: Theory and Experiment. *Phys. Rev. B* **2011**, *83*, 245415.

(26) Kepenekian, M.; Le Guennic, B.; Robert, V. Primary Role of the Electrostatic Contributions in a Rational Growth of Hysteresis Loop in Spin-Crossover Fe(II) Complexes. *J. Am. Chem. Soc.* **2009**, *131*, 11498–11502.

(27) Barth, J. V. Fresh Perspectives for Surface Coordination Chemistry. *Surf. Sci.* **2009**, *603*, 1533–1541.

(28) Carbone, C. et al. Self-Assembled Nanometer-Scale Magnetic Networks on Surfaces: Fundamental Interactions and Functional Properties. *ChemPhysChem* **2011**, *21*, 1212–1228.

(29) Gambardella, P. et al. Supramolecular Control of the Magnetic Anisotropy in Two-dimensional High-spin Fe Arrays at a Metal Interface. *Nature Mater.* **2009**, *8*, 189–193.

(30) Umbach, T. R.; Bernien, M.; Hermanns, C. F.; Krüger, A.; Sessi, V.; Fernandez-Torrente, I.; Stoll, P.; Pascual, J. I.; Franke, K. J.; Kuch, W. Ferromagnetic Coupling of Mononuclear Fe Centers in a Self-Assembled Metal-Organic Network on Au(111). *Phys. Rev. Lett.* **2012**, *109*, 267207.

(31) Abdurakhmanova, N.; Tseng, T.-C.; Langner, A.; Kley, C. S.; Sessi, V.; Stepanow, S.; Kern, K. Superexchange-Mediated Ferromagnetic Coupling in Two-Dimensional Ni-TCNQ Networks on Metal Surfaces. *Phys. Rev. Lett.* **2013**, *110*, 027202.

(32) Giovanelli, L.; Savoyant, A.; Abel, M.; Maccherozzi, F.; Ksari, Y.; Koudia, M.; Hayn, R.; Choueikani, F.; Otero, E.; Ohresser, P.; Themlin, J.-M.; Dhesi, S. S.; Clair, S. Magnetic Coupling and Single-Ion

Anisotropy in Surface-Supported Mn-Based Metal-Organic Networks. *J. Phys. Chem. C* **2014**, *118*, 11738–11744.

(33) Faraggi, M. N.; Golovach, V. N.; Stepanow, S.; Tseng, T.-C.; Abdurakhmanova, N.; Kley, C. S.; Langner, A.; Sessi, V.; Kern, K.; Arnau, A. Modeling Ferro- and Antiferromagnetic Interactions in Metal-Organic Coordination Networks. *J. Phys. Chem. C* **2015**, *119*, 547–555.

(34) Umbach, T. R.; Bernien, M.; Hermanns, C. F.; Sun, L. L.; Mohrmann, H.; Hermann, K. E.; Krüger, A.; Krane, N.; Yang, Z.; Nickel, F.; Chang, Y.-M.; Franke, K. J.; Pascual, J. I.; Kuch, W. Site-specific Bonding of Copper Adatoms to Pyridine End Groups Mediating the Formation of Two-dimensional Coordination Networks on Metal Surfaces. *Phys. Rev. B* **2014**, *89*, 235409.

(35) Gütlich, P.; Garcia, Y.; Goodwin, H. A. Spin Crossover Phenomena in Fe(II) Complexes. *Chem. Soc. Rev.* **2000**, *29*, 419–427.

(36) Murray, K. S.; Kepert, C. J. Cooperativity in Spin Crossover Systems: Memory, Magnetism and Microporosity. *Top. Curr. Chem.* **2004**, *233*, 195–228.

(37) Spiering, H. Elastic Interaction in Spin Crossover Compounds. *Top. Curr. Chem.* **2004**, *235*, 171–195.

(38) Kepenekian, M.; Le Guennic, B.; Robert, V. Magnetic Bistability: From Microscopic to Macroscopic Understandings of Hysteretic Behavior Using Ab initio Calculations. *Phys. Rev. B* **2009**, *79*, 094428.

(39) El Hajj, F.; Sebki, G.; Patinec, V.; Marchivie, M.; Triki, S.; Handel, H.; Yefsah, S.; Tripier, R.; Gómez-García, C. J.; Coronado, E. Macrocycle-Based Spin-Crossover Materials. *Inorg. Chem.* **2009**, *48*, 10416–10423.

(40) Stock, P.; Deck, E.; Hohnstein, S.; Korzekwa, J.; Meyer, K.; Heinemann, F. W.; Breher, F.; Hörner, G. Molecular Spin Crossover in Slow Motion: Light-Induced Spin-State Transitions in Trigonal Prismatic Iron(II) Complexes. *Inorg. Chem.* **2016**, *55*, 5254–5265.

(41) Blakesley, D. W.; Payne, S. C.; Hagen, K. S. Spin-State Variation in Solid State and Solution of Mononuclear Iron(II) 1,4,7-Trimethyl-1,4,7-triazacyclonane Complexes. *Inorg. Chem.* **2000**, *39*, 1979–1989.

(42) Reger, D. L.; Gardinier, J. R.; Gemmill, W. R.; Smith, M. D.; Shahin, A. M.; Long, G. J.; Rebbouh, L.; Grandjean, F. Formation of Third Generation Poly(pyrazolyl)borate Ligands from Alkyne Coupling

Reactions of Fe[(p-IC6H4)B(3-Rpz)3]2 (R) H, Me; pz) Pyrazolyl): Pathways toward Controlling an Iron(II) Electronic Spin-State Crossover. *J. Am. Chem. Soc.* **2005**, *127*, 2303–2316.

(43) Halcrow, M. A. The Spin-states and Spin-transitions of Mononuclear Iron(II) Complexes of Nitrogen-donor Ligands. *Polyhedron* **2007**, *26*, 3523–3576.

(44) Lebègue, S.; Pillet, S.; Angyan, J. G. Modeling Spin-crossover Compounds by Periodic DFT+ U approach. *Phys. Rev. B* **2008**, *78*, 024433.

(45) Kepenekian, M.; Robert, V.; Le Guennic, B.; de Graaf, C. Energetics of [Fe(NCH)6]2+ Via CASPT2 Calculations: A Spin-Crossover Perspective. *J. Comput. Chem.* **2009**, *30*, 2327–2333.

(46) Fumanal, M.; Jiménez-Grávalos, F.; Ribas-Arino, J.; Vela, S. Lattice-Solvent Effects in the Spin-Crossover of an Fe(II)-Based Material. The Key Role of Intermolecular Interactions between Solvent Molecules. *Inorg. Chem.* DOI: 10.1021/acs.inorgchem.7b00017.

(47) Soler, J. M.; Artacho, E.; Gale, J. D.; García, A.; Junquera, J.; Ordejón, P.; Sánchez-Portal, D. The SIESTA Method for *Ab Initio* Order-N Materials Simulation. *J. Phys.: Condens. Matter* **2002**, *14*, 2745–2779.

(48) Artacho, E.; Anglada, E.; Diéguez, O.; Gale, J. D.; García, A.; Junquera, J.; Martin, R. M.; Ordejón, P.; Pruneda, J. M.; Sánchez-Portal, D.; Soler, J. M. The SIESTA Method; Developments and Applicability. *J. Phys.: Condens. Matter* **2008**, *20*, 064208.

(49) Dion, M.; Rydberg, H.; Schröder, E.; Langreth, D. C.; Lundqvist, B. I. Van der Waals Density Functional for General Geometries. *Phys. Rev. Lett.* **2004**, *92*, 246401.

(50) Klimeš, J.; Bowler, D. R.; Michaelides, A. Chemical Accuracy for the van der Waals Density Functional. *J. Phys.: Condens. Matter* **2010**, *22*, 022201.

(51) Bengtsson, L. Dipole Correction for Surface Supercell Calculations. *Phys. Rev. B* **1999**, *59*, 12301–12304.

(52) Dudarev, S. L.; Botton, G. A.; Savrasov, S. Y.; Humphreys, C. J.; Sutton, A. P. Electron-energy-loss Spectra and the Structural Stability of Nickel Oxide: An LSDA+U Study. *Phys. Rev. B* **1998**, *57*, 1505–1509.

(53) Vela, S.; Fumanal, M.; Ribas-Arino, J.; Robert, V. Towards an Accurate and Computationally-efficient Modelling of Fe(II)-based Spin Crossover Materials. *Phys. Chem. Chem. Phys.* **2015**, *17*, 16306.

(54) Troullier, N.; Martins, J. L. Efficient Pseudopotentials for Plane-Wave Calculations. *Phys. Rev. B* **1991**, *43*, 1993–2006.

(55) Artacho, E.; Sánchez-Portal, D.; Ordejón, P.; García, A.; Soler, J. M. Linear-Scaling *Ab-Initio* Calculations for Large and Complex Systems. *Phys. Status Solidi B* **1999**, *215*, 809–817.

(56) Tersoff, J.; Hamann, D. R. Theory and Application for the Scanning Tunneling Microscope. *Phys. Rev. Lett.* **1983**, *50*, 1998–2001.

(57) Tersoff, J.; Hamann, D. R. Theory of the Scanning Tunneling Microscope. *Phys. Rev. B* **1985**, *31*, 805–813.

(58) Bocquet, M.-L.; Lesnard, H.; Monturet, S.; Lorente, N. In *Computational Methods in Catalysis and Materials Science*; van Santen, P., R. A. & Sautet, Ed.; Wiley-VCH, 2009.

(59) Bader, R. F. W.; Henneker, W. H.; Cade, P. E. Molecular Charge Distributions and Chemical Binding. *J. Chem. Phys.* **1967**, *46*, 3341–3363.

(60) Tang, W.; Sanville, E.; Henkelman, G. A Grid-based Bader Analysis Algorithm Without Lattice Bias. *J. Phys.: Condens. Matter* **2009**, *21*, 084204.

(61) Kresse, G.; Furthmüller, J. Efficiency of Ab-initio Total Energy Calculations for Metals and Semiconductors Using a Plane-wave Basis Set. *Comput. Mat. Sci.* **1996**, *6*, 15–50.